Materials Chemistry and Physics 255 (2020) 123510

Contents lists available at ScienceDirect

Materials Chemistry and Physics

journal homepage: www.elsevier.com/locate/matchemphys

Photo-induced electrical behavior under gas adsorption on SnO_2 -based heterostructures

Diego H.O. Machado [a], José H.D. da Silva [a], Fabrício T. Russo [a], Luis V.A. Scalvi [a,*]

[a] UNESP, São Paulo State University, Department of Physics, FC and Graduate Program in Materials Science and Technology (POSMAT), Bauru, SP, Brazil

HIGHLIGHTS

- Investigation of photo-induced electrical transport under gas influence in SnO_2.
- Influence of Er^{3+} surface ions on adsorption of charged oxygen species.
- Photo-induced room temperature effects on gas adsorption in heterostructures.

ARTICLE INFO

Keywords:
Tin dioxide
Gallium arsenide
Heterostructure
Electrical transport
Gas sensing

ABSTRACT

Er-doped SnO_2 thin films are produced by a combined technique where films are deposited by resistive evaporation from a precursor powder obtained by sol-gel. Films are deposited on different substrates and analyzed concerning the electrical conduction on different directions. The film conductivity (parallel to the surface) changed significantly when exposed to light, even though the photon energies are below the SnO_2 bandgap energy (InGaN LED, 2.75 eV). The SnO_2 films present distinct trapping characteristics when exposed to oxygen or carbon monoxide, in agreement with the behavior of metallic oxides, suggesting that surface defects act as adsorption sites. The photo-excitation is rather lower for a GaAs/SnO_2 heterostructure sample where the GaAs layer is deposited by sputtering, since the direction of polarization (through the interface barrier, perpendicular to the sample surface) does not lead to significant increase in the sample current. When the bottom layer is a GaAs crystal wafer, the current magnitude increases drastically under the InGaN LED excitation. The results reported here contribute to the understanding of electrical transport and the influence of gas adsorption on evaporated SnO_2 films deposited in diverse configurations on distinct substrates, and contributes to gas sensing applications.

1. Introduction

Tin dioxide has wide application in gas sensors, because it is sensitive to many sort of gases, including reducing gases (e.g. acetone, hydrogen, ethanol, methanol, carbon monoxide, nitrogen monoxide, ammonia and hydrogen sulfide) and oxidizing gases (e.g. oxygen, nitrogen dioxide, H_2O_2, H_2SO_4, ozone). Many of reducing and oxidizing gases can also be toxic gases (CO, NO_2, H_2S, NH_3) [1,2]. Good efficiency has been found more recently for SnO_2 gas sensors in the form of nanoparticles [3–7]. This referenced gas sensors are based on undoped tin oxide nanoparticles, which present low sensitivity and long response-recovery time. It is related to fact the that SnO_2 nanoparticles tend to agglomerate easily, making it difficult to diffuse gas molecules on the semiconductor surface [3]. The material surface area and the shape of agglomerates present on the surface strongly influence the gas detection performance. Small size, large surface area and uniformly dispersed nanoparticles can easily adsorb gas molecules and improve gas detection properties [3].

Recently, many different techniques have been used to produce advanced SnO_2 geometries and shapes. As examples, SnO_2:Rh nanofibers were produced by electro-spinning technique [7], SnO_2 nanosheets were prepared by hydro-solvethermal treatment [8], Pt-decorated SnO_2 nanoneedles were synthesized by hydrothermal method [9] and Au/SnO_2/RGO nanocomposites, with SnO_2 nanoparticles, were prepared by one-step wet chemical method [10]. These geometries for SnO_2 gas sensors have shown improvements in gas sensor

* Corresponding author.
E-mail address: luis.scalvi@unesp.br (L.V.A. Scalvi).

https://doi.org/10.1016/j.matchemphys.2020.123510
Received 3 March 2020; Received in revised form 18 June 2020; Accepted 30 June 2020
Available online 22 July 2020

properties for distinct gases such as carbon monoxide, acetone, formaldehyde and ethanol. Another interesting feature concerns the use of light to induce improvements in the sensor performance A close-packed SnO_2 monolayer array film composed of nanospheres with hollow structure was used as sensing platforms under UV-light irradiation, and exhibited excellent sensing performances for NO_2 gas with a detection limit of 100 ppb [11]. An ultrafast response/recovery speed at room temperature is also obtained. A visible-light activated room temperature gas sensor based on perylenediimide (PI)/SnO_2 nanoparticles heterojunctions show significantly enhance the sensing performance for NO_2 detection with high sensitivity and high selectivity [12]. Amorphous $ZnSnO_3$ shows outstanding UV sensitivity and gas-sensing property at room temperature [13] which can be combined in order improve the efficiency. In general, gas sensors based on optimized and modern geometries such as WO_3 nanocrystals, ZnO nanowires, In_2O_3 or SnO_2 nanoparticles have good performance, but have some disadvantages such as high operating temperature (in the range 170–200 °C for H_2 and about 200 °C for CO detection), leading to high power consumption and integration difficulty [4,5].

Many techniques have been explored to deposit tin oxide thin films, among them: dip and spin-coating via sol gel [2,14–17] and resistive evaporation [14,17,18]. The latter method has some advantages such as large deposition area, multilayer structure deposition and rather lower cost when compared to other techniques such as pulsed laser deposition (PLD) and molecular beam epitaxy (MBE). In this work, SnO_2 films were produced by a combination of two thin film deposition methods: the solution is produced by the sol-gel route and the thin film deposition is accomplished by the resistive evaporation technique, using the powder obtained from drying the sol-gel solution.

Concerning the incorporation of Er^{3+} in the SnO_2 matrix, in addition to providing luminescence, it increases the material resistivity when compared to undoped films, as Er^{3+} ions replace Sn^{4+} in the SnO_2. This substitution leads to charge compensation with free electrons, originated from the naturally n-type matrix, as Er^{3+} ions act as acceptors. Another effect that occurs when incorporating trivalent rare earth ions is the increase in intergranular potential barrier densities per unit area, since the dopant decreases the crystallite size [19], increasing the crystallites concentration. The resulting effect is a decrease in the electronic mobility of the material [20]. Then, both effects: the reduction in free carier concentration and the reduced mobility contribute to an effective lower conductivity.

The presence of traps in SnO_2 is very common and plays a fundamental role in the sample electrical performance. A capture barrier is evaluated from a model for photo-induced conductivity, the same sort of experiment used here, yielding 100 meV forSnO_2:0.1% Er and 148 meV for SnO_2:4% Er, suggesting defects with lattice relaxation between distinct charged states [21]. More recent and advanced geometries of SnO_2 matrix also reveal the relevance of trapped charge. Nanoflowers geometry is characterized by a lower density of surface traps in the bandgap since they present very high crystallinity [22]. Consequently SnO_2 nanoflowers have higher Fermi energy and higher conductivity, since more electrons populate the conduction band.

Decay of photoinduced conductivity has already been performed for GaAs/SnO_2 heterojunctions, however, GaAs films were deposited by resistive evaporation and SnO_2 was deposited by sol-gel dip coating on the GaAs layer. Electron capture was observed due to intra-bandgap defects in the SnO_2 layer, as well as possible electron trapping at the GaAs/SnO_2 interface at temperatures below 100 K. In addition to Eu^{3+} centers (the rare-earth doping used in that report) and oxygen vacancies, this heterostructure also had areas of Eu^{3+} clusters on the surface of the SnO_2 layer, contributing to electron scattering [23]. Measurement of photoinduced current decay may also be performed in a gaseous atmosphere, with optical excitation concomitant with the change of atmosphere. For the heterojunction of SnO_2:Sb with TiO_2 in O_2 atmosphere, an improvement in the gas detection properties performance after illumination was observed, contributing to increase the adsorption centers on the surface of the exposed TiO_2 layer [24].

In the present work, distinct light sources (He–Ne laser and InGaN LED) are used to excite carriers concomitant with gas adsorption on the top SnO_2 surface, and the current decay is exploited using the decay of the photo-induced conductivity. It is expected that the InGaN LED can excite SnO_2 intra-bandgap defects, and electron-hole pairs and defect states in GaAs, since the photon energy is low enough to penetrate to the bottom layer. The aim of this work is the contribution to understanding of the combination of photoexcitation and distinct gas atmospheres to the electrical transport in evaporated SnO_2 deposited onto distinct substrates. We expect that the knowledge on the combination of photo-induced electrical transport under distinct gas adsorption helps in the design of gas sensing applications with operation at room temperature, in the near future.

2. Experimental

2.1. Samples production

The sol-gel solution of tin dioxide was produced by using $ErCl_3$ added to SnO_2 solution, in the appropriate proportion, to form SnO_2:1 at%Er^{3+}. It was accomplished by mixing pentahydrate tin tetrachloride ($SnCl_4{\cdot}5H_2O$) and erbium chloride ($ErCl_3$), to obtain a final concentration of 1 at% Er in relation to tin dioxide. In this solution, concentrated NH_4OH was added until the pH was raised to 11. The suspension was placed in semipermeable membranes, subjected to dialysis against distilled water for approximately ten days, in order to eliminate Cl^- and NH^{4+} ions, so that the final pH of the solution is approximately 7. Once the solution was ready, the SnO_2: Er powder was obtained by evaporating the solvent from the sol-gel solution, and then, using the powder in the resistive evaporation procedure. The deposition was carried out in a self-purpose built system with a resistive molybdenum crucible as the evaporation vessel. SnO_2 films were deposited on soda-lime glass, a-SiO_2, sputtered GaAs film (heterostruture GaAs/SnO_2) and onto GaAs wafer crystal grown using vertical temperature gradient freezing method (VGF), fabricated by Wafer World Inc., Florida, as described in Table 1. The residual pressure in the evaporation chamber was about 10^{-5} torr. The evaporated samples deposited on glass were thermally annealed at 300 °C, films deposited onto a-SiO_2 substrate were treated at 1000 °C, as also described in Table 1, while films deposited on GaAs (both forms) were not annealed. Table 1 summarizes the conditions for obtaining the SnO_2 samples deposited by resistive evaporation on different surfaces, and corresponding labels. Some basic characterization data using this combination of sol-gel route and resistive evaporation technique was published recently [25]. The samples illustration (SnO_2 thin film and heterojunction GaAs/SnO_2) is shown in Fig. 1.

2.2. Current excitation and decay under gas influence

Samples were introduced in an adapted cryostat which allows gas incidence upon manipulation correct of valves. The reported data in this paper are obtained according to the following procedures, which are better visualized in Fig. 2: 1) a fixed potential (a voltage of 30 V was

Table 1
Samples used in this paper: SnO_2 deposited at different surfaces and with distinct thermal annealing.

Sample Name	Substrate	Annealing temperature/time
S10(*)	a-SiO_2	1000 °C/1 h
S3(*)	Soda lime glass	300 °C/5 h
HET1(**)	a-SiO2 (on a sputtered GaAs film)	as deposited
HET2(***)	VGF grown wafer	as deposited

* Model can be seen in Fig. 1 top left.
** Model can be seen in Fig. 1 top right.
*** Model can be seen in Fig. 1 bottom.

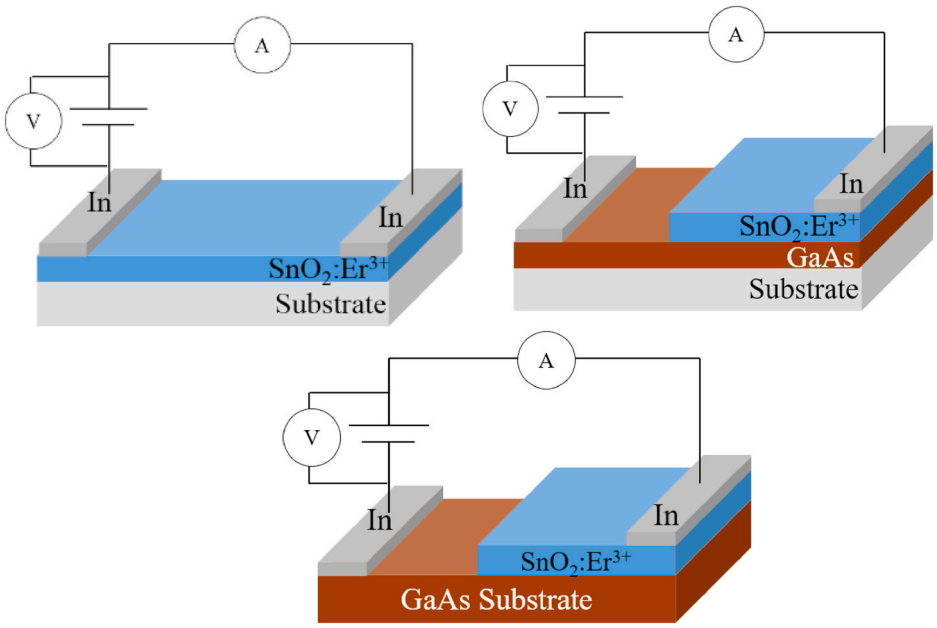

Fig. 1. Sample representations: (top left) evaporated SnO_2 films/soda-lime or silica glass substrates; (top right) GaAs/SnO_2 films deposited heterostructure; (bottom) heterostructure of SnO_2 film on VGF GaAs substrate wafer.

chosen for all samples) is applied on the samples, under vacuum conditions (about 10^{-4} Torr) until the current becomes stable. The current through the sample is measured parallel to the surface, according to Fig. 1 (top left) for samples S3 and S10, using a Keithley electrometer model 6517A. For the heterostructure samples (HET1 and HET2), the current is measured perpendicular to the sample surface, according to Fig. 1 (top right and bottom). The voltage is applied using the voltage source of the same Keithley device. As the measured current was stable, the vacuum was sealed and the desired gas was released in the system, in the dark. The current was monitored over a period of time (Fig. 2(a)); 2) Concerning the procedure involving light irradiation, a stable signal of electric current in the sample was again awaited and after that, the sample was irradiated with a light source. During the process the current is monitored until it reaches 5 min of excitation by the light source. At this time the current practically reaches saturation in most of the situations. Then, this excitation time was fixed as standard for all the measurements. At the same moment that the illumination of the sample is removed, the desired gas is released into the system or not, while the current decay is measured over a period of time, according to Fig. 2(b).

These electrical characterization measurements were then, carried in different atmospheres: vacuum, CO_2-rich or O_2-rich, performed for 1% Er^{3+} doped SnO_2 evaporated films and GaAs/SnO_2:1% Er^{3+} heterostructure (HET1). It is worth mentioning that the system pressure when inserting the gas was 1 atm, as verified in the gas pressure meter. It is expected because the gas fills completely the cryostat chamber, almost instantaneously.

Concerning the normalization procedure, it consists in dividing all the measured values of current by the maximum value just before allowing the gas inside the chamber. In the case of high light excitation the maximum normalized value is 1, because light irradiation is removed concomitant with gas release. However, in the cases where light does not causes a high influence (or in the dark), the maximum value may be higher than 1, which means that the gas injection may increase slightly the initial conductivity.

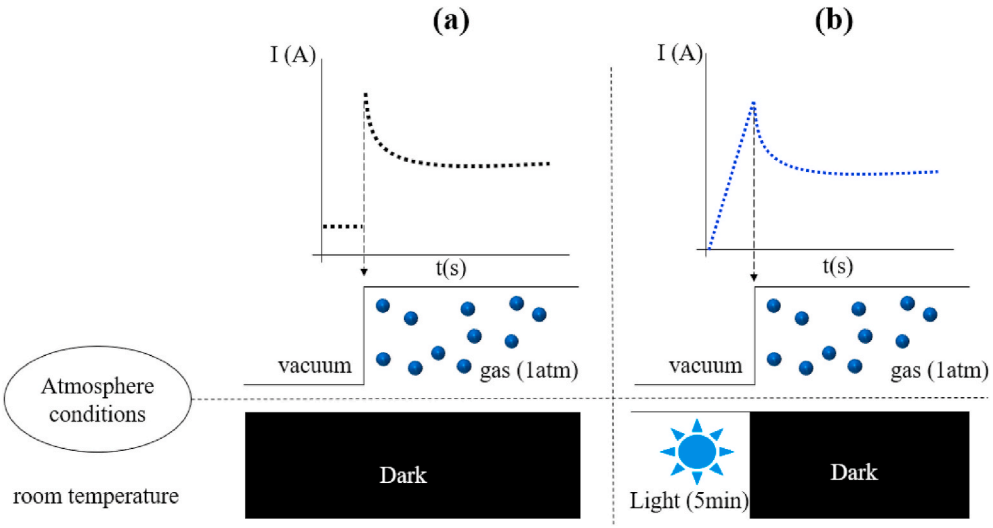

Fig. 2. Representation of the experimental procedure of the current as a function of time under O_2 and CO_2 atmospheres influence (a) without light excitation and (b) light excitation.

2.3. Scanning electron microscopy

Scanning electron microscopy (SEM) and X-ray dispersive energy (EDX) measurements were performed on heterostructure samples on a scanning electron microscope of Carl Zeiss model LS15. Before the measurements, a thin layer of gold was deposited on the sample surface to avoid charging effect and as consequence it prevents distortion on the images.

3. Results and discussion

3.1. SnO_2 evaporated thin films

Fig. 3(a) shows normalized current-time data measured in the dark under three distinct atmospheres: vacuum, 1 atm of CO_2 or 1atm of O_2, for sample S10. The inset of this figure shows the measurement in actual values of current. Applied voltage is 30V, leading to very low values of current, in the order of nA. Note that prior to time "zero" the sample is maintained under vacuum conditions. Fig. 3 (b) and (c) present the excitation and decay of the photoinduced current for sample S10 performed under the same three conditions of Fig. 3(a): vacuum, CO_2 or O_2 atmosphere, but in this case concomitant with photoexcitation using the He–Ne laser and the InGaN LED sources, respectively. The inset in Fig. 3 (c) displays actual current values. It is important to notice the magnitude of the current after excitation with the InGaN LED (inset of Fig. 3(c)), since the current values are about 12 times the value in the dark, for the time zero of decay process. This result assures that the LED has an intense effect in the electrical transport excitation, even though the photon energy is below the bandgap energy of SnO_2. Then, only intra-bandgap states are excited, and no electron-hole pair creation is expected in the SnO_2 layer.

Results of excitation and decay for all the samples reported in this paper are summarized in Table 2, at the end of this section. Allowing gas incidence in the initial vacuum conditions of the S10 sample, leads to an initial increase in the conductivity for CO_2 and O_2 atmospheres, corresponding to stimulus of 2.0% for O_2 and 2.4% for CO_2, in the electrical conduction with a instant response to gases. After the initial increase, the electrical conduction decreases more slowly corresponding to 0.7% and 1.2% for O_2 and CO_2 atmospheres, respectively, about 50 s after the initial increase, which is stabilization time of the sample current. Quick stimulus was also obtained by Z. Jie et al. [6] analyzing response and recovery time of SnO_2 films exposed to acetone and alcohols. In that case this response time is related to fast reaction rate between acetone and adsorbed oxygen species. It suggests the existence of chemisorbed negative oxygen ions on the surface of the SnO_2 film. The presence of previously adsorbed charged oxygen is also relevant for CO_2 adsorption, as discussed below. In the case of Table 2, the electrical conductivity of SnO_2 decreases considerably when exposed to oxygen, although O_2 adsorption is low, as expected from metal oxides. This suggests that only surface defects act as adsorption sites. In addition, adsorbed species can

Table 2
Photo-induced excitation and current decays under different atmospheres, represented in terms of the percentage change in conductivity.

			S10 (%)	S3 (%)	HET1 (%)
Dark	Excitation	O_2	2.0	7.3	0.4
		CO_2	2.4	8.6	0.6
	Decay	O_2	0.7	9.8	1.1
		CO_2	1.2	9.9	1.7
He–Ne	Excitation	O_2	2.1	1.6	0.4
		CO_2	5.8	–	0.3
	Decay	O_2	0.9	7.9	1.1
		CO_2	4.7	2.0	0.9
InGaN	Excitation	O_2	721	100	6.1
		CO_2	676	144	5.4
	Decay	O_2	8.2	16.4	3.7
		CO_2	21.6	22.1	3.1

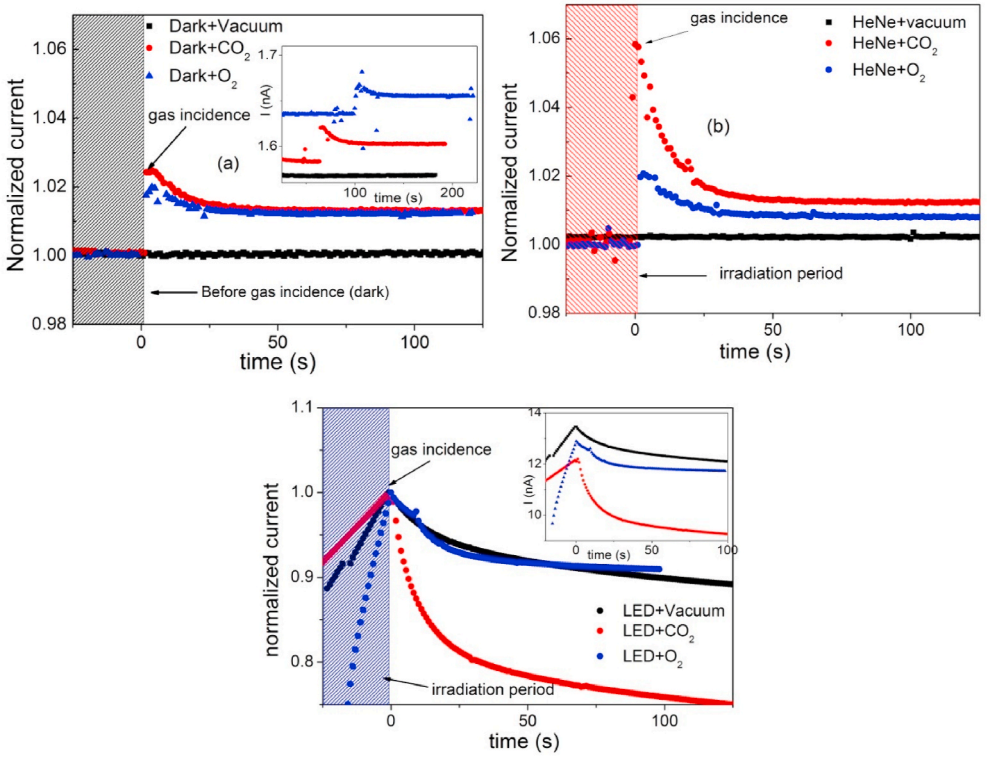

Fig. 3. Excitation and normalized decay of current as a function of time under different conditions for sample S10: (a) in the dark and vacuum, and under influence of CO_2 and O_2 atmospheres. Inset: actual current values, applied voltage: 30 V; (b) same atmosphere conditions, but excited with He–Ne laser and (c) same atmosphere conditions, but excited by InGaN LED. Inset: actual current values.

be attributed to various forms of oxygen adsorption such as O_2, O_2^-, O^- and O^{2-} [26]. Even in the case of CO_2 adsorption, the presence of previously adsorbed charged oxygen forms is necessary to accomplish the adsorption of oxygen dioxide [27–29]. The sensor resistance varies under exposition to CO_2, which depends on the reaction between the surface oxygen species and gaseous CO_2 molecules.

Leite and coworkers [30] observed that Nb_2O_5 doped SnO_2 nanoparticles presents shorter response time and higher conductivity than pure SnO_2 films when using gaseous ethanol to test the device. As in this case, the films had a signal stability after a certain time under the controlled atmosphere. Chowdhuri and collaborators also reported [31] that resistance decreases with time when films of SnO_2 spread with CuO nanoparticles on the surface, are subjected to the atmosphere of 20 ppm of H_2S, being more efficient for gas detection than undoped SnO_2 film. This is the opposite of our case since H_2S and ethanol are reducing agents (oxide sample has resistance decrease with time) whereas O_2 and CO_2 are oxidizing agents (resistance increase with time).

Fig. 3(b) and (c) shows photo-induced excitation and decay of the photoinduced current for sample S10 performed under vacuum, and in a CO_2 or O_2 atmosphere, in this case with concomitant photoexcitation using the He–Ne laser (628 nm) and the InGaN LED (450 nm) respectively. The experimental procedure was described in the previous section and be summarized as follows: while still in vacuum the sample was illuminated (with one of the light sources mentioned above) for 5 min. Given the elapsed time, the illumination was turned off and at this very same moment either CO_2 or O_2 gas was released into the system chamber.

Although both sources have energy below the SnO_2 bandgap, the sample response is quite different. When excited with the He–Ne laser, the S10 sample has behavior similar to the one in the dark, with CO_2 gas stimulus being slightly higher than O_2 stimulus (Table 2). The decay in this case is similar to the dark, although slightly higher: 4.7% in CO_2 and 0.9% in O_2. The irradiation with the InGaN LED leads to a very effective carrier generation with average excitation of 7 times higher compared to the dark conductivity. In this case, the observed decay is 21.6% for CO_2 and 8.2% for O_2, taking into account the 50-s interval after gas incidence (current stabilization time). This result shows that, although both light sources have energies below the SnO_2 bandgap, the InGaN LED has a higher influence on sample excitation, ionizing intrabandgap states with higher intensity. Moreover, it is evident that, regardless of the light source, the CO_2 gas has much more significant influence on electron capture in the sample.

It can be seen in Fig. 3 (b) and (c) that as the light source energy is being irradiated on the sample, there is an increase in its conduction, and the maximum value of the current obtained for excitation with the InGaN LED was 13.45 nA (about 7 times higher compared to the dark current), whereas for the He–Ne laser it was 1.77 nA (5.8% higher than the dark current). These light sources release electrons in the device, primarily from the SnO_2 surface states to the conduction band, leaving out positively charged sites that will be able to adsorb oxygen molecules in the form of negatively charged O_2^-, O_2^- or O^- species [26]. Gaseous species that are adsorbed on the SnO_2 surface, as time goes by, capture electrons from the conduction band and as consequence, the conductivity decreases. Electron capture is governed by intra-bandgap defects, which have been optically ionized. CO_2 species are more effective for this purpose as shown in Fig. 3(c), where the decay rate in CO_2 atmosphere is much more efficient. It seems that the presence of previously adsorbed charged oxygen forms is also necessary to accomplish the adsorption of carbon dioxide, as recently reported [27,29]. The resistance increase (conductivity decreases) for long times, observed in Fig. 3, is related to reaction of CO_2 molecules with adsorbed charge oxygen species on the surface, which comes from the air and are not completely eliminated. However, the exact mechanism of room temperature interaction under the presence of light is still an issue for future investigation.

Fig. 4 shows scanning electron microscopy (SEM) for samples S3 and S10. It is clearly observed that there is an increase in the sample roughness with increase in the annealing temperature.

The adsorption of oxygen causes the granular surface of the n-type SnO_2 to be covered with negatively charged oxygen particles [32], as schematically shown in Fig. 5. It leads to electron trapping from the SnO_2 bulk, leading to the formation of a charged layer at the SnO_2 grain boundary, concomitant with a potential barrier at the grain interface. Based on this phenomenon, the gas sensor ends up operating with high resistance, and in this case, the effect seen is the decrease of sample conduction after a certain time exposed to the air or specific gas atmosphere [32]. Concerning Fig. 5 it is clear that the rougher the surface, as is the case of sample S10 [25], more charged oxygen species are adsorbed, since the surface area becomes larger. However, looking Table 2, the variation on conductivity is higher for sample S3, which means that the Er doping is playing an important role. As we have published recently, the Er^{3+} species are mainly located close to surface sites for lower annealing temperatures [25]. The sole exception for this trapping behavior is the excitation with the InGaN LED (Table 2), which is consistent with the relative presence of Er^{3+} species on substitutional sites [25]. The implications concerning roughness and Er^{3+} distribution will be treated again below.

Fig. 6 shows normalized current values as function of time, with the real current value being plotted in the inset, performed under vacuum, or under CO_2 and O_2 rich atmosphere for sample S3 being performed in the dark or under irradiation of He–Ne laser and InGaN LED light sources respectively, a similar procedure done to sample S10 (Fig. 3). The sample S3 has a decay rate of 9.9% for CO_2 and 9.8% for O_2 for dark measurements; 2% for CO_2 and 7.9% for O_2 after He–Ne laser irradiation and decay rate of 22.1% for CO_2 and 16.4% for O_2 after 5-min excitation by the InGaN LED. It is also important to mention that the excitation by the InGaN LED is much lower in this case compared to S10 sample, being about 7 times higher in the case of the sample with higher annealing temperature.

When excited with the LED, the excitation energy (average 2.75V) is close to the excitation energy of transitions from level $^4I_{15/2}$ to levels $^4F_{5/2}$ (2.74eV) and $^4F_{3/2}$ (2.79eV) of Er^{3+} ions [33] that suggests that this light source may excite ions in the S10 sample more efficiently. In the S10 sample Er^{3+} ions populate preferentially substitutional sites whereas asymmetric boundary layer sites are determinant for sample S3 [25], and harder to be efficiently excited, justifying the higher photo-induced conductivity of the S10 sample, after InGaN LED excitation.

Small oscillations in the current value shown in Fig. 6(b) for CO_2 atmosphere are due to the mechanical instabilities of the system (it was necessary to open the gas valve causing disturbance (vibrations) in the cryostat during the measurement, and as consequence, there was a brief fluctuation in the current value.

As mentioned, sample S10 has higher photo-induced conduction when compared to S3, but except for the He–Ne excitation under CO_2 atmosphere, the S3 sample has a better trapping response to CO_2 and O_2 gas atmosphere when compared to the S10 sample (Table 2). It may be related to the Er^{3+} ions distribution close to the sample surface, as represented in Fig. 5 which is substantially different in these two sorts of samples. It has been observed in a recent publication [25] that as the annealing temperature increases, the concentration of Er surface ions decreases, as consequence of diffusion into the sample bulk. For the ions located more inside the sample in symmetric substitutional sites, as the case of the sample thermally annealed at 1000 °C (S10), the InGaN LED has more efficiency in the excitation, as already shown in this paper, and in excellent agreement with the mentioned publication [25]. However, although more difficult to be excited, the more surface located Er^{3+} ions in the S3 sample represents easier charge location for interaction with the oxygen gaseous species in the surface, explaining the more efficient trapping and the larger reduction on conduction with time for the S3 sample, even though the S10 has rougher surface (Fig. 4), which makes easier the gas path on the surface. Larger surface area and well-dispersed

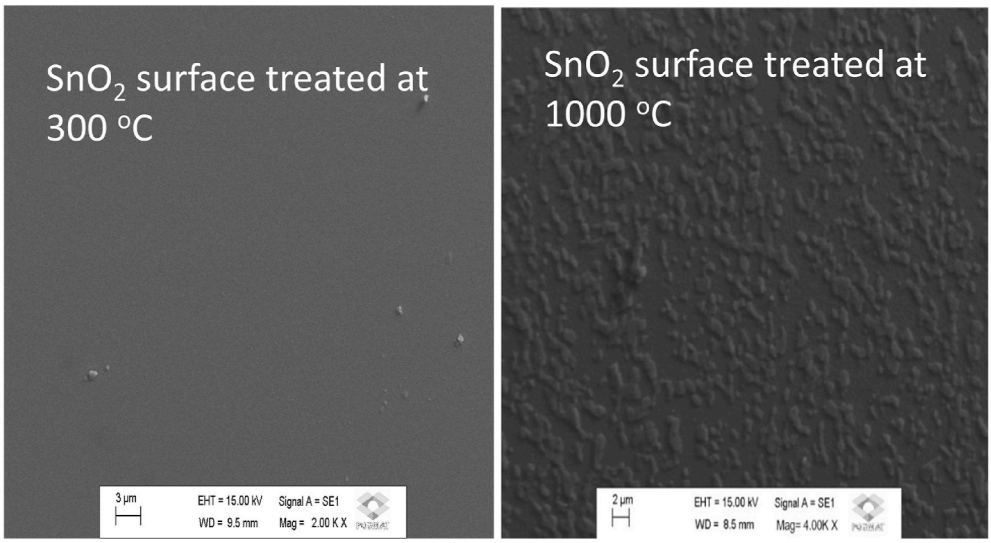

Fig. 4. Surface SEM of evaporated Er^{3+}-doped SnO_2: (left) annealed at 300 °C (S3) (right) annealed at 1000 °C (S10).

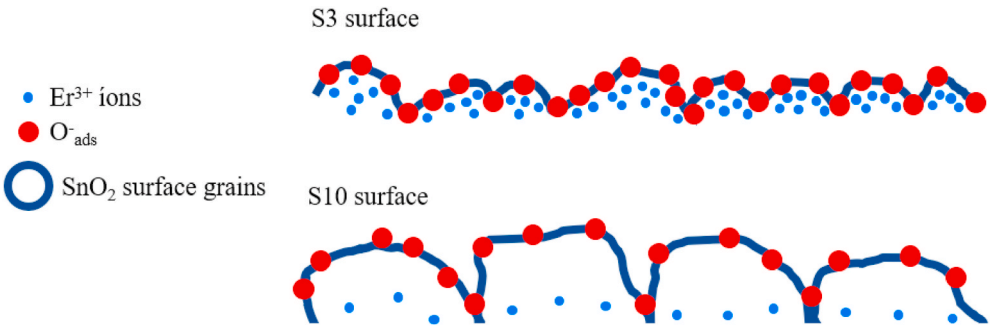

Fig. 5. Schematic diagram of evaporated SnO_2 thin films surface, with Er^{3+}ions and negatively charged oxygen adsorbed species distribution.

nanoparticles contribute to the adsorption of gas molecules and improve gas detection properties [3]. However, the presence of Er^{3+} in a location highly dependent on the thermal annealing temperature seems to be reversing this rule.

It is well known that the electrical conductivity of SnO_2 will increase when exposed to reduced gases such as methane, ammonia and hydrogen sulfide, however, it will decrease in the oxidizing gas atmosphere, such as oxygen [5]. This phenomenon has been observed in the present work for both SnO_2 samples: S3 and S10. As already discussed, the rutile structure of SnO_2 has oxygen vacancies and interstitial tin atoms, causing some defects in the lattice [2,18]. Since these sorts of defects contribute to the conductivity they shall participate directly to the gas detection property. In other words, SnO_2 with more oxygen vacancies generally has higher sensitivity for gas detection [5]. Then, the presence of both: oxygen vancancies and surface Er^{3+} are significant to the transport properties and may help the design of a gas sensor based on SnO_2 conductivity.

3.2. *Influence of gas and light on heterostrucuture GaAs/SnO_2*

As seen in Fig. 1, the layout is quite different for this sample, which presents conduction measured in the growth direction. Consequently the current is much higher, which is related to the area of conduction. Fig. 7 shows scanning electron microscopy (SEM) image of HET1 sample surface, along with a sample sketched diagram. The left side of the image is composed of GaAs and the right side is the SnO_2 film. Apparently, for this magnitude of amplification, both layers are homogeneous and smooth, without agglomerations. The separation between these layers is clearly seen. Fig. 8 brings 10 times more amplification than Fig. 7, containing in (a) is the SEM of the GaAs surface and in (b) the SnO_2 surface. The GaAs layer remains regular and it can be seen that it is actually smoother than SnO_2, which has some irregularities. The HET1 sample has an evaporated SnO_2 film above an amorphous GaAs film, what may be causing an increase in the tension between SnO_2 and GaAs. Since these materials have different crystalline structures as a result it may be causing the observed surface irregularities in SnO_2.

Fig. 9 shows X-ray dispersive energy (EDX) scanning on the surface of sample HET1, corresponding to the SEM image shown in Fig. 7. In the top left figure, it can be seen the surface distribution of elements Sn and O placed together. In the other images (right and bottom), it is shown the individual distribution of each element, for the analyzed area (O in green and Sn in red). A uniform distribution of Sn (in red) and O (in green) elements are identified, with higher concentration located at the right side of each figure. The small amount of green and red dots respectively, on the left side of these figures is related to the noise background of the measurement. Considering that the SnO_2 film was deposited only at the right part of the figure, as seen in Fig. 7, no dot should be found in the opposite side. For this reason the amount of Er, which is much smaller, is masked, avoiding a precise identification in this case, unlike previously published for similar samples [25].

Current-voltage measurements were performed for the GaAs/SnO_2 heterostructure sample (HET1), either in the dark or under the effect of different light sources (He–Ne laser and InGaN LED), and also under gas incidence. These measurements indicated ohmic behavior in the dark as well as under the influence of light sources, independent on light source used or gaseous atmosphere. However, no significant differences were

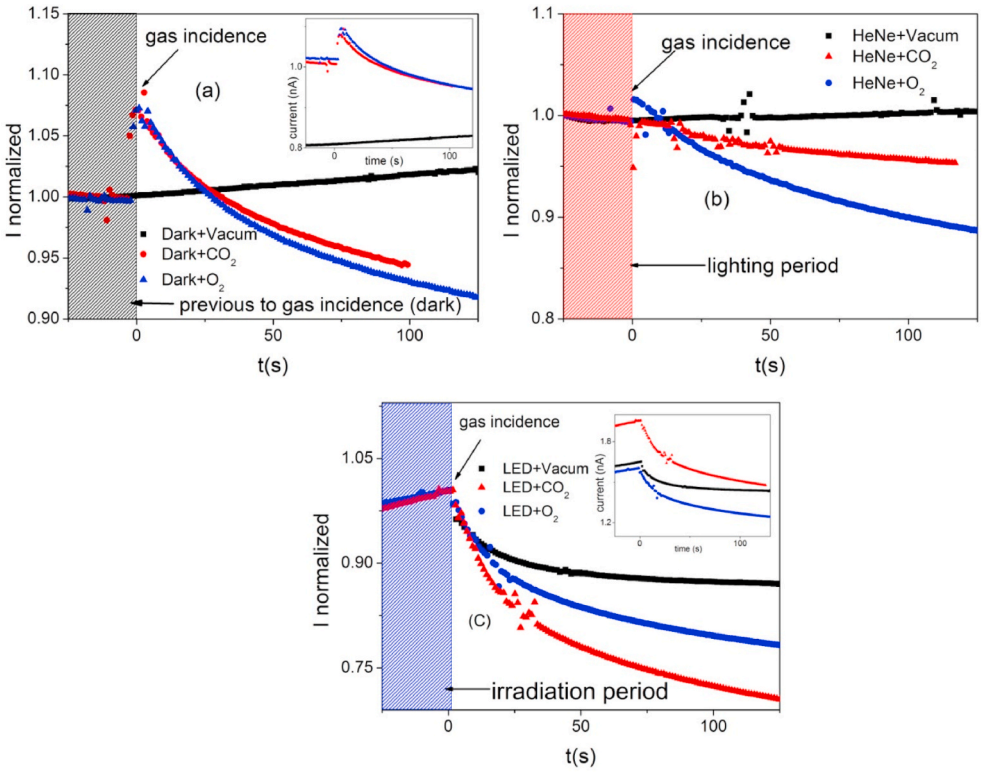

Fig. 6. Excitation and normalized decay of current as a function of time under different conditions for sample S3: (a) in the dark and vacuum, and under influence of CO_2 and O_2 atmospheres. **Inset:** actual current values, applied voltage: 30 V; (b) same atmosphere conditions, but excited with He–Ne laser and (c) same atmosphere conditions, but excited by InGaN LED. Inset: actual current values.

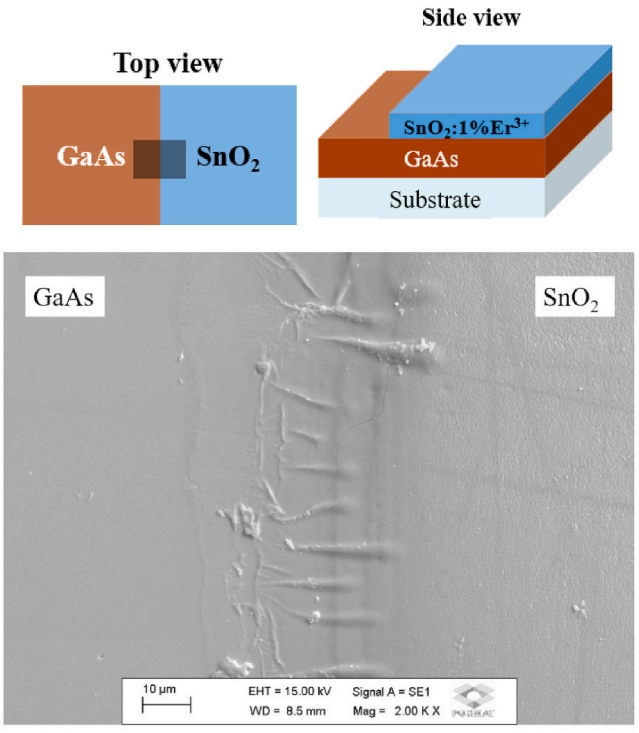

Fig. 7. (top) schematic diagram of the HET1 sample. (bottom) Surface SEM of HET1 sample.

noticed when comparing measurements performed in the dark with those performed with incidence of light or gaseous atmosphere. The effect of these different forms of excitation, although quite significant, is rather fast as shown in Fig. 10, below. Then, this I–V data were not reproduced here.

Fig. 10 shows normalized current-time data measured in the dark under vacuum conditions, or 1 atm CO_2 or O_2 atmosphere for sample HET1. In the inset of this figure, it is shown the measurement in actual values of current. Applied voltage is 30V leading to values of current, in the order of microAmps.

It is important to mention that the responses of SnO_2 films (S3 and S10) and the heterostructure (HET1), although different, occur at room temperature, which is difficult to observe in SnO_2-based gas sensors, generally operating at elevated temperatures [5,34]. As easily observable in Fig. 8, the evaporated SnO_2 has rougher surface compared with GaAs sputtered film. This is opposite when the tin oxide is evaporated on GaAs substrate [25] and, then, the irregular surface observed for the sample HET1, where SnO_2 is deposited on top of a sputtered GaAs film, may contribute to gas detection. Besides, the absence of thermal annealing leads to a high concentration of Er^{3+} ions on the surface, as already discussed for evaporated SnO_2 samples, and shown schematically in Fig. 5. This also improves the efficiency on gas detection.

As already mentioned, both light sources used here have energy above the GaAs bandgap energy (1.97eV for He–Ne laser and 2.75 eV for InGaN LED), but cause small stimulation in the GaAs/SnO_2 heterostructure sample, which suggests that the radiation do not reach the GaAs layer, since the top is made up of SnO_2. The HET1 sample showed a decay rate of 1.1% in O_2 atmosphere and 1.7% for CO_2 (both in the dark) and 1.05% for O_2 and 0.9% for CO_2 when excited with the HeNe laser. As shown in Figs. 3 and 6, SnO_2: 1% Er^{3+} samples also showed small decay rate, except for InGaN LED excitation, which leads to much more efficient trapping rates. In this case, the rates were 21.6% and 22.1% for samples S10 and S3, respectively, when exposed to CO_2, in opposition to what happens in the HET1 samples where the decay rate are 3.7% in O_2 and 3.1% in CO_2. Although it could lead to erroneously think of poor efficiency, it has actually to do with conductivity direction, since in this

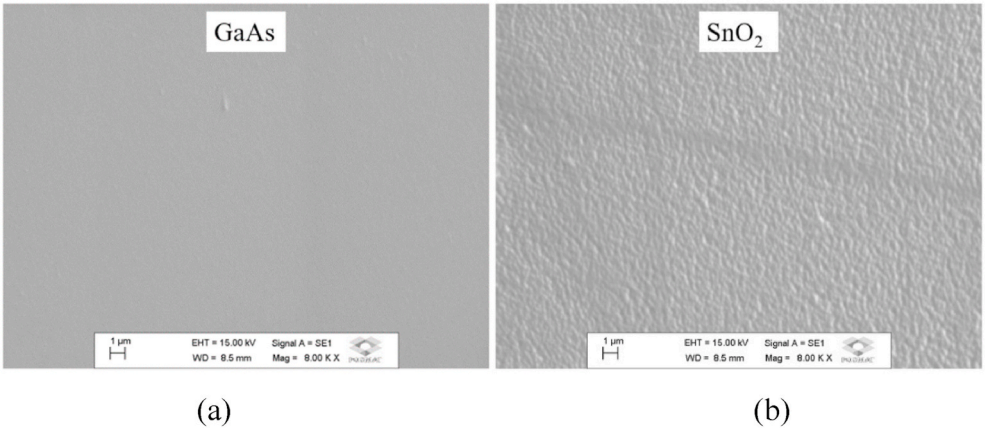

Fig. 8. Surface SEM of HET1 sample where a) GaAs thin film and b) SnO_2:1%atEr^{3+} evaporated thin film (on GaAs film).

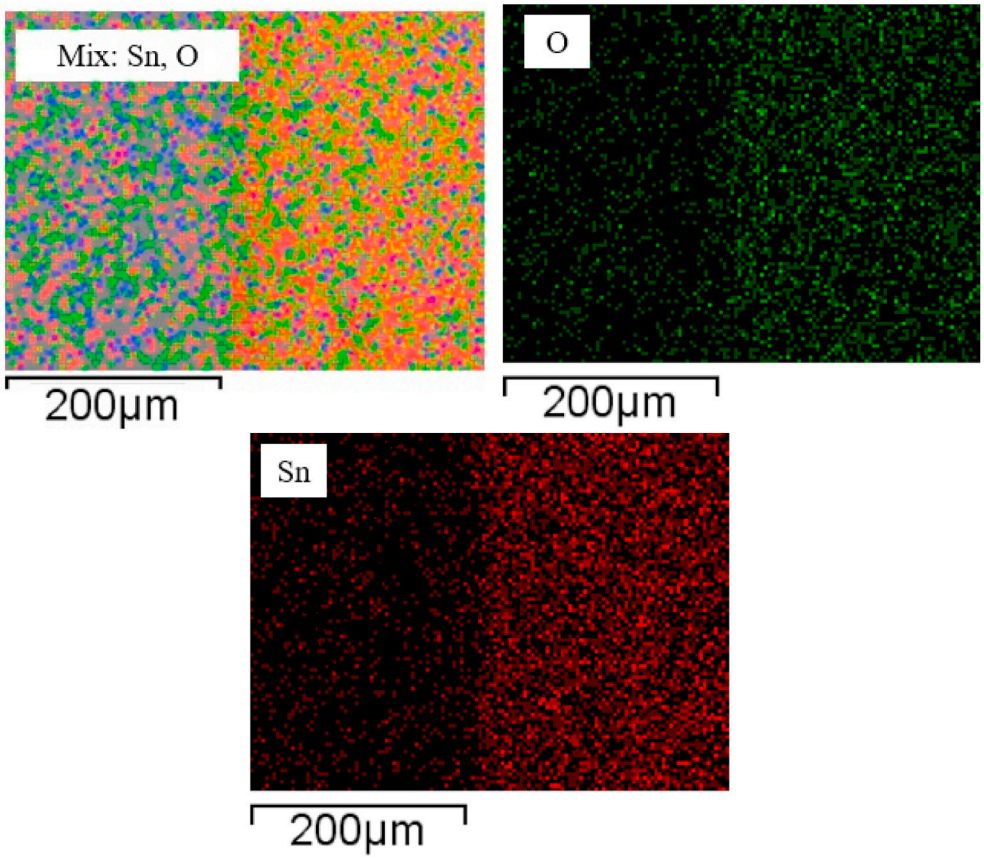

Fig. 9. Scanning EDX for HET1 sample.

case the barrier between both layers shall play as main parameter for improving conduction. Probably, the high n-type conductivity in SnO_2 makes the photo induced carrier excitation not enough to increase significantly the conduction, and no significant increase is produced in a sample that is already ohmic in the dark, not exhibiting the expected rectifying behavior. Besides, the current magnitude is higher because the conducting area is much larger when compared to the conduction along with the SnO_2 thin layer in samples S3 and S10.

However, the GaAs/SnO_2:1%Er^{3+} heterostructure stabilizes in a shorter time compared to the evaporated SnO_2:1% Er^{3+} thin films. For SnO_2 samples and the HET1 heterostructure sample, the He–Ne laser did not cause any excitation, probably because this laser does not have the energy required to excite the Er^{3+} ions. As noted before for evaporated SnO_2 samples [25], the InGaN LED was able to excite these ions more efficiently as the excitation energy of the InGaN LED light source, as already mentioned, is close to the excitation energy of the Er^{3+} transitions from level $^4I_{15/2}$ to levels $^4F_{5/2}$ and $^4F_{3/2}$ [25,33].

Fig. 11(a) shows current voltage behavior at two different temperatures for sample HET2, and Fig. 11(b) is the SEM for the interface in the sample surface. The doped SnO_2 film is deposited directly on top of VGF grown GaAs (single crystalline). The symmetric rectifying behavior is as expected and the current clearly increases with temperature. The inset in Fig. 11(a) shows the excitation with the InGaN LED in this sample for three different temperatures, under applied voltage of 20V. The lines are drawn just as guide to the eyes. As can be seen the light source leads to an increase of four orders of magnitude in the current, assuring the very

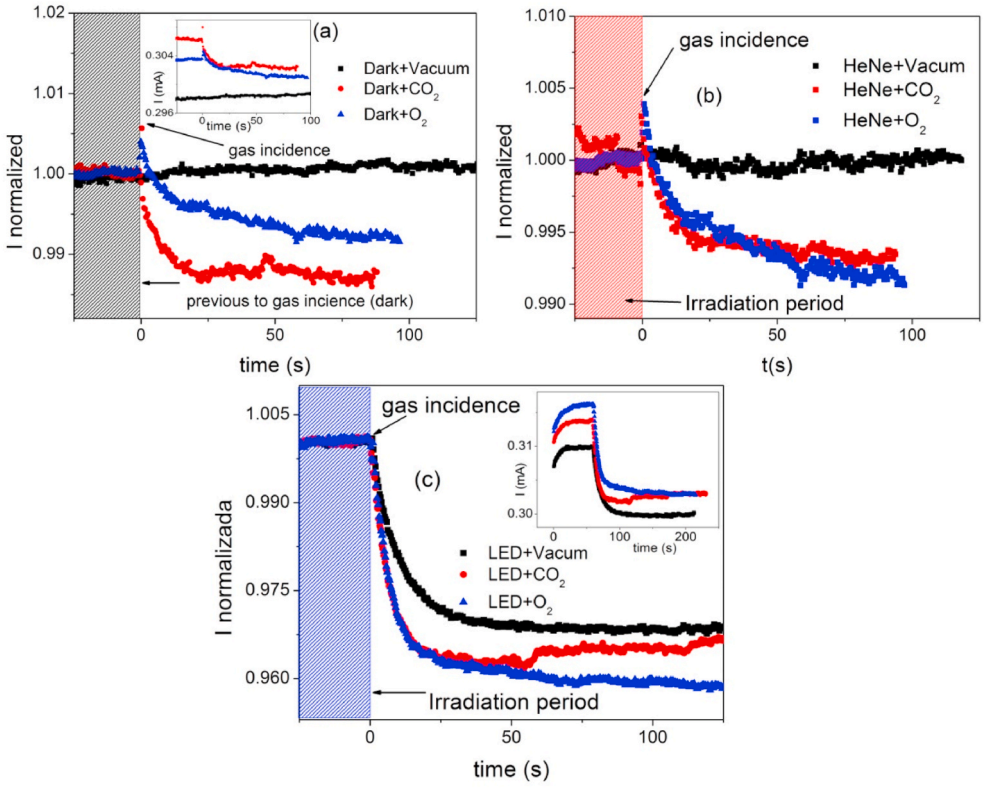

Fig. 10. Excitation and normalized decay of current as a function of time under different conditions for heterostructure sample HET1: (a) in the dark and vacuum, and under influence of CO_2 and O_2 atmospheres. Inset: actual current values, applied voltage: 30 V; (b) same atmosphere conditions, but excited with He–Ne laser and (c) same atmosphere conditions, but excited by InGaN LED. Inset: actual current values.

high efficiency of the blue light source to this sort of heterostructure, and the transparency of the SnO_2 layer for it, making sure that electron-hole pairs are excited very efficiently in the GaAs single crystalline layer. It is important to mention that in this case the current magnitude returns to the dark value immediately after removing the light source incidence.

In order to compare the excitation of samples HET1 and HET2, the diagram of Fig. 12 is sketched. Values of bandgap, represented in this figure, were evaluated by the Tauc Plot [35] from optical transmittance data. Considering the quite high electron concentration in the SnO_2 side [36], there is an electron distribution, with top energy above the interface barrier energy. Although the InGaN LED source is enough to excite the Er^{3+} ion in both sort of samples, the excitation of the single crystalline GaAs layer is much more efficient, as observed for the HET2 sample (Er-doped SnO_2 on top of VGF grown GaAs), assuring much higher magnitude when compared to HET 1 sample (SnO_2 layer on top of sputtered GaAs). The rather fast decay after light removal in the case of HET2 may lead to a possible improvement in gas detection, since the instrumentation is developed to follow the decay. However, the current magnitude is so high in this case that electron capture by gaseous species may not lead to measurable exchanges in the electrical transport through the barrier.

4. Conclusion

Measurements of excitation and decay of photoinduced current in different atmospheres showed that the electrical conductivity of Er-doped evaporated SnO_2 films changed significantly when exposed to oxygen and carbon monoxide, in agreement with the behavior of metallic oxides, suggesting that surface defects act as adsorption sites. The electron trapping may be increased by exciting with below SnO_2 bandgap light source energy (2.75 eV). Gaseous species that are adsorbed on the surface of the SnO_2, capture conduction band electrons and the conductivity decreases over time. Er^{3+} ions are located close to the surface in the case of low thermal annealing temperature or in the bulk substitutional sites, in the case of high annealing temperature. These ions have strong contribution in the gaseous adsorption process, and then, in the time-dependent conductivity.

The excitation is rather lower for a GaAs/SnO_2 heterostructure sample where the GaAs layer is deposited by sputtering, because the direction of polarization (through the interface barrier), does not lead to significant increase in the sample current under gas influence. When the bottom layer is a VGF grown GaAs layer the current magnitude increases drastically under InGaN LED excitation (above GaAs bandgap light). The effect caused by the gas adsorption is less than the observable for SnO_2 layer, where the polarization is perpendicular to the growth direction (parallel to sample surface).

This work is a contribution to understanding of the combination of photoexcitation and distinct gas atmospheres to the electrical transport in evaporated Er-doped SnO_2 deposited on several configurations with distinct substrates. The knowledge developed so far on the distinct GaAs/SnO_2 sample design contributes to room temperature gas sensing applications in the near future.

Credit author statement

D. H. O. Machado is responsible for depositing the samples and performing most of the experiments. J. H. D. da Silva has given support for the resistive evaporation of SnO_2 samples and heterostructures, and very relevant contributions for the discussion on electrical characterization results. F. T. Russo is responsible for the experiments with the HET2 sample and very significant contributions on O_2 and CO_2 adsorption processes. L. V. A. Scalvi has helped with the experimental setup and interpretation of results concerning gas adsorption measurements, and coordinated the project. All authors were engaged in the

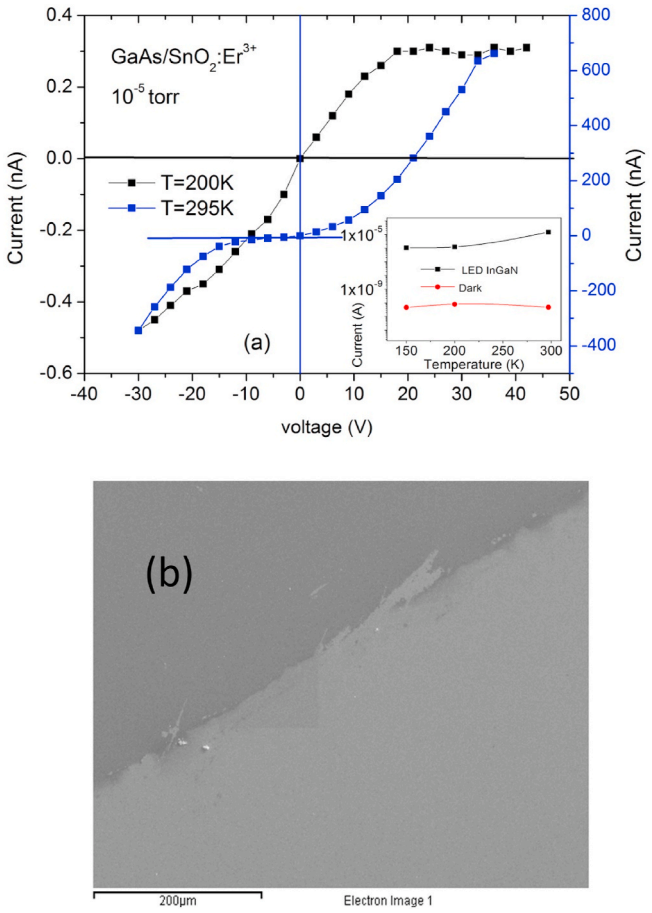

Fig. 11. (a) Current-Voltage for sample HET2 at 200 K and 295 K, under vacuum, in the dark. Inset: InGaN LED (450 nm) excitation on this sample as function of temperature. (b) Scanning electron microscopy for sample HET2.

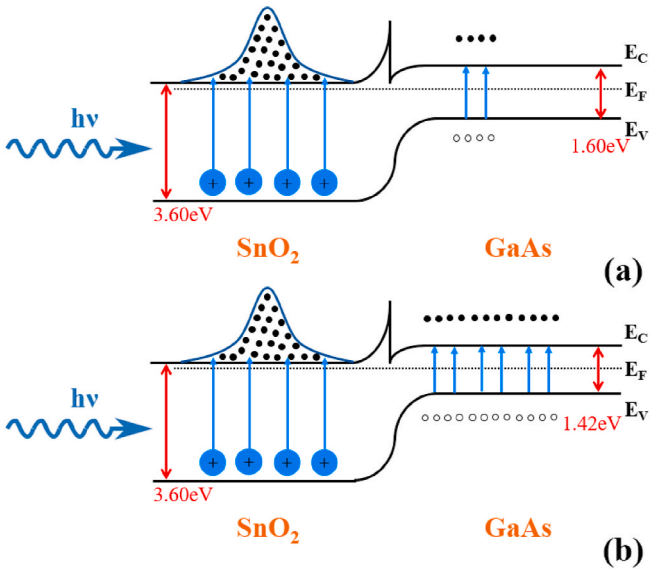

Fig. 12. Schematic diagram showing the excitation of electron-hole pairs in GaAs and Er^{3+} ions, that promote electron transfer to the SnO_2 conduction band. (a) Gas deposited by sputtering (b) GaAs wafer grown by VGF.

writing of the manuscript.

Declaration of competing interest

The authors declare that they have no known competing financial interests or personal relationships that could have appeared to influence the work reported in this paper.

Acknowledgements

We would like to thank financial support from CAPES, CNPq, and FAPESP (grants 2016/12216-6 and 2017/18916-2).

Appendix A. Supplementary data

Supplementary data to this article can be found online at https://doi.org/10.1016/j.matchemphys.2020.123510.

References

[1] G.E. Patil, D.D. Kajale, D.N. Chavan, N.K. Pawar, P.T. Ahire, S.D. Shinde, V. B. Gaikwad, G.H. Jain, Synthesis, characterization and gas sensing performance of SnO_2 thin films prepared by spray pyrolysis, Bull. Mater. Sci. 34 (2011) 1–9.
[2] S.M. Al-Jawad, A.K. Elttayf, A.S. Saber, Influence of annealing temperature on the characteristics of nanocrystalline SnO_2 thin films produced by sol–gel and chemical bath deposition for gas sensor applications, Surf. Rev. Lett. 24 (2017) 1750104.
[3] Y. Chang, Y. Yao, B. Wang, H. Luo, T. Li, L. Zhi, Reduced graphene oxide mediated SnO_2 nanocrystals for enhanced gas-sensing properties, J. Mater. Sci. Technol. 29 (2013) 157–160.
[4] H. Zhang, J. Feng, T. Fei, S. Liu, T. Zhang, SnO_2 nanoparticles-reduced graphene oxide nanocomposites for NO_2 sensing at low operating temperature, Sensor. Actuator. B Chem. 190 (2014) 472–478.
[5] L. Li, S. He, M. Liu, C. Zhang, W. Chen, Three-dimensional mesoporous graphene aerogel-supported SnO_2 nanocrystals for high-performance NO_2 gas sensing at low temperature, Anal. Chem. 87 (2015) 1638–1645.
[6] J. Zhao, L.H. Huo, S. Gao, H. Zhao, J.G. Zhao, Alcohols and acetone sensing properties of SnO_2 thin films deposited by dip-coating, Sensor. Actuator. B Chem. 115 (2006) 460–464.
[7] X. Kou, N. Xie, F. Chen, T. Wang, L. Guo, C. Wang, Q. Wang, J. Ma, Y. Sun, H. Zhang, G. Lu, Superior acetone gas sensor based on electrospun SnO_2 nanofibers by Rh doping, Sensor. Actuator. B Chem. 256 (2018) 861–869.
[8] G. Li, Z. Cheng, Q. Xiang, L. Yan, X. Wang, J. Xu, Bimetal PdAu decorated SnO_2 nanosheets based gas sensor with temperature-dependent dual selectivity for detecting formaldehyde and acetone, Sensor. Actuator. B Chem. 283 (2019) 590–601.
[9] Q. Zhou, L. Xu, A. Umar, W. Chen, R. Kumar, Pt nanoparticles decorated SnO_2 nanoneedles for efficient CO gas sensing applications, Sensor. Actuator. B Chem. 256 (2018) 656–664.
[10] F. Meng, M. Li, C. Wang, Y. Sun, One-step synthesis of Au/SnO_2/RGO nanocomposites and their VOC sensing properties, IEEE Trans. Nanotechnol. 17 (2018) 212–219.
[11] B. Liu, Y. Luo, K. Li, H. Wang, L. Gao, G. Duan, Room-temperature NO_2 gas sensing with ultra-sensitivity activated by ultraviolet light based on SnO_2 monolayer array film, Adv. Mater. Interfaces 6 (2019) 1900376.
[12] X. Tian, X. Yang, F. Yang, T. Qi, A visible-light activated gas sensor based on perylenediimide-sensitized SnO_2 for NO_2 detection at room temperature, Colloids Surf., A 578 (2019) 123621.
[13] X. Wang, et al., Preparation of transparent amorphous $ZnSnO_3$ cubic nanoparticles and light-induced homostructures: application in UV sensor and room- temperature gas sensor, Appl. Surf. Sci. 493 (2019) 862–872.
[14] H. Kim, R.C.Y. Auyeung, A. Piqué, Transparent conducting F-doped SnO_2 thin films grown by pulsed laser deposition, Thin Solid Films 516 (2008) 5052–5056.
[15] D. Leng, L. Wu, H. Jiang, Y. Zhao, J. Zhang, W. Li, L. Feng, Preparation and properties of SnO_2 film deposited by magnetron sputtering, Int. J. Photoenergy (2012) 1–6, 2012.
[16] F.H. Aragón, V.A. Chitta, J.A.H. Coaquira, P. Hidalgo, H.F. Brito, Long-range ferromagnetic order induced by a donor impurity band exchange in SnO_2:Er^{3+}nanoparticles, J. Appl. Phys. 114 (2013) 203902.
[17] O.A. Hussein, N.A. Ali, Effect of capillary tube on structural and optical properties of SnO_2 thin films prepared by, APCVD 10 (2017) 202–207.
[18] S. Das, V. Jayaraman, SnO, A comprehensive review on structures and gas sensors, Prog. Mater. Sci. 66 (2014), 112–255.
[19] E.A. Morais, L.V.A. Scalvi, S.J.L. Ribeiro, V. Geraldo, Poole-Frenkel effect in Er doped SnO_2 thin films deposited by sol-gel-dip-coating, Phys. Status Solidi 202 (2005) 301–308.
[20] T.T.T. Van, S. Turrell, B. Capoen, Le Van Hieu, M. Ferrari, Davor Ristic, L. Boussekey, C. Kinowski, Environment segregation of Er^{3+} emission in bulk sol-gel-derived SiO_2-SnO_2 glass ceramics, J. Mater. Sci. 49 (2014) 8226–8233.
[21] E.A. Morais, L.V.A. Scalvi, Decay of photo-excited conductivity of Er-doped SnO_2 thin films, J. Mater. Sci. 42 (2007) 2216–2221.

[22] N.K. Elumalai, R. Jose, P.S. Archana, V. Chellappan, S. Ramakrishna, Charge transport through electrospun SnO_2 nanoflowers and nanofibers: role of surface trap density on electron transport dynamics, J. Phys. Chem. C 116 (2012) 22112–22120.
[23] C.F. Bueno, L.V.A. Scalvi, Electron trapping in the photo-induced conductivity decay in GaAs/SnO_2 heterostructure, Appl. Phys. A 124 (2018) 457, 2018.
[24] R.A. Ramos, M.H. Boratto, L.V.A. Scalvi, On the photo-induced electrical conduction related to gas sensing of the Sb: SnO_2/TiO_2 heterostructure, Sens. Actuat. A Phys. 281 (2018) 250–257.
[25] D.H.O. Machado, J.H.D. Silva, A. Tabata, L.V.A. Scalvi, Influence of thermal annealing on the properties of evaporated Er-doped SnO_2, Mater. Res. Bull. 120 (2019) 110585.
[26] N. Yamazoe, J. Fuchigami, M. Kishikawa, T. Seiyama, Interactions of tin oxide surface with O_2, H_2O and H_2, Surf. Sci. 86 (1979) 335–344.
[27] T.V.K. Karthik, L. Martinez, V. Agarwal, Porous silicon ZnO/SnO2 structures for CO_2 detection, J. Alloys Compd. 731 (2018) 853–863.
[28] M. Melle-Franco, G. Pacchioni, A.V. Chadwick, Cluster and periodic ab initio calculation on the adsorption of CO_2 on the SnO_2 (110) surface, Surf. Sci. 478 (2001) 25–34.
[29] D. Wang, Y. Chen, Z. Liu, L. Li, C. Shi, H. Qin, J. Hu, CO_2-sensing properties and mechanism of nano-SnO_2 thick- film sensor, Sensor. Actuator. B 227 (2016) 73–84.
[30] E.R. Leite, I.T. Weber, E. Longo, J.A. Varela, A new method to control particle size and particle size distribution of SnO_2 nanoparticles for gas sensor applications, Adv. Mater. 12 (2000) 965–968.
[31] A. Chowdhuri, V. Gupta, K. Sreenivas, R. Kumar, S. Mozumdar, P.K. Patanjali, Response speed of SnO_2-based H_2S gas sensors with CuO nanoparticles, Appl. Phys. Lett. 84 (2004) 1180–1182.
[32] Y. Shimizu, SnO_2 Gas Sensor, in: G. Kreysa, K. Ota, R.F. Savinell (Eds.), Encyclopedia of Applied Electrochemistry, Springer, New York, NY, 2014, pp. 1974–1982.
[33] C. Bouzidi, A. Moadhen, H. Elhouichet, M. Oueslati, Er^{3+}-doped sol-gel SnO_2 for optical laser and amplifier applications, Appl. Phys. B Laser Optic. 90 (2008) 465–469.
[34] Y.C. Zhang, L. Yao, G. Zhang, D.D. Dionysiou, J. Li, X. Du, One-step hydrothermal synthesis of high-performance visible-light-driven SnS_2/SnO_2 nanoheterojunction photocatalyst for the reduction of aqueous Cr(VI), Appl. Catal. B Environ. 144 (2014) 730–738.
[35] J. Tauc, Optical properties and electronic structure of amorphous Ge and Si, Mater. Res. Bull. 3 (1968) 37–46.
[36] V. Geraldo, L.V.A. Scalvi, P.N. Lisboa-Filho, C. Morilla-Santos, Drude's model calculation rule on electrical transport in Sb-doped SnO_2 thin films, deposited via sol–gel, J. Phys. Chem. Solid. 67 (2006) 1410–1415.